Characteristics of asymmetric turbulent near wakes

Nakayama, Akihiko

Kreplin, Hans-Peter

(Citation)
Physics of Fluids,6(7):2430-2439

(Issue Date)
1994-07

(Resource Type)
journal article

(Version)
Version of Record

(URL)
https://hdl.handle.net/20.500.14094/90001175

Characteristics of asymmetric turbulent near wakes

Akihiko Nakayama
Faculty of Engineering, Kobe University, Rokkodai, Nada-ku, Kobe, 657 Japan

Hans-Peter Kreplin
German Aerospace Research Establishment (DLR), Bunsenstrasse 10, D-37073 Goettingen, Germany

(Received 31 March 1993; accepted 24 February 1994)

The mean-velocity and turbulence quantities in a few qualitatively different types of asymmetric two-dimensional turbulent near wakes in nearly zero-pressure gradient have been experimentally studied. In all cases, the log-law similarity of the boundary layers was found to continue into the initial part of the wake, with the same similarity variables as in the boundary layers on the same side, provided the origin of the normal distance is taken at the smooth extension of the respective surfaces. The Reynolds stress profiles show sharp peaks just downstream of the trailing edge, and the magnitudes of the peaks are found to be related to the values of the surface friction at the trailing edge. These peaks grow into the full width of the wake to form the far wake profiles. In this process, the turbulent diffusions of the Reynolds stresses are very important, and when the size asymmetry is severe, is not clearly of the gradient-transport type.

I. INTRODUCTION

Computation of high-Reynolds number turbulent flows around streamlined bodies must include calculation of the wake flows as well as the boundary layer flows, both of which require appropriate turbulence models. The near wake region requires an accurate model, since it is the trailing-edge region that plays a decisive role in the determination of the entire flow and the lift. While a great many studies have been made to device methods that can predict boundary layer flows accurately in various situations, corresponding efforts on wake flows are scarce. Often, methods verified in the boundary layers are adapted without scrutinizing. It has been found, however, in computations of airfoil boundary layers and their wakes (Tulapurkara *et al.*[1] and Henau *et al.*[2] for example), that a turbulence model that works for boundary layers does not necessarily work in the wake and efforts to refine the model are being made (for example, Kim and Chung[3] and Spalart and Allmaras[4]). When the wake is highly asymmetric and curved, as in the case of a body experiencing high lift, which results from merging of a very thick boundary layer on the suction-surface side, and thin and accelerated boundary layer on the pressure side, requirements for an acceptable model is severe, and more work is needed.

At the trailing edge of a streamlined body, where the boundary layers transform into a wake, the skin friction suddenly drops to zero, and at the same time, the wall restriction on the normal-to-wall velocity component is removed. In symmetric wakes, this allows turbulent mixing across the wake centerline and initiates the inner wake.[5] In asymmetric wakes, both mean flow and turbulent transport across the wake centerline take place. Therefore, the relative intensities and the relative size of the turbulence from two sides become important in the development. In addition, there is a longer-range influence due to equalization of the pressure field, when there is a pressure variation in the trailing-edge region, as in the case of airfoil experiencing lift. In general, these effects appear as combined and interact with each other.

Asymmetry obtained by roughening one side of a flat plate has been studied by Andreopoulos and Bradshaw[5] in detail. The roughness increases the thickness and the skin friction, but hardly changes the shape of the velocity profile. The type of asymmetry seen in the wake of airfoils and other streamlined bodies can be very different from asymmetry, just in the size. The boundary layer on one side may be very close to separation, while that on the other side may be strongly accelerated, so that the characteristics of the boundary layers are very different. Leuchter[6] studied asymmetric wakes generated downstream of a flat plate by contouring the ceiling and the floor of the tunnel differently. The asymmetry obtained in this way is somewhat closer to the airfoil wake, but is mild and makes the external flow itself asymmetric. Thompson and Whitelaw[7] and Badri Narayanan *et al.*,[8] on the other hand, used a resistance such as a screen to retard the flow on one side of the body. The asymmetric flow obtained this way is more like a mixing layer between two streams of different total pressures, and they show wake-like behavior only in the region very close to the trailing edge, and quickly start to show the mixing-layer type profiles.

In the present work, we study the effects of more general asymmetry in the initial part of the wake, but with minimum direct influence of pressure gradients. For this purpose, pairs of boundary layers with different properties were generated using a deformable plate model and the characteristics of the asymmetric near wake resulting from the merging of these boundary layers were examined. Specifically, the similarity of the velocity profiles, development of the turbulent stresses, and triple products are examined in detail. One drawback of keeping the pressure nearly constant in the trailing edge region and downstream is that the boundary layer at the trailing edge tends to be those returning to the flat-plate boundary layers, but it is better than having complicating effects of the pressure gradients. The work is intended to clarify how the velocity profile similarity and the development of Reynolds stresses and their transports are influenced by the asymmetry. The results will also provide a guideline for turbulence modeling, particularly practical methods based on the Reynolds-averaged equations, but the results

 1070-6631/94/6(7)/2430/10/$6.00

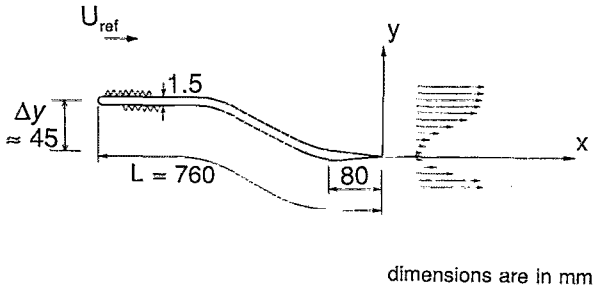

FIG. 1. Sketch of the model.

can provide ideas about similarity that can also be used, for example, in large-eddy simulations. Some details of the general properties of the flow are also given for the purpose of validating computational methods. All data are available on floppy disks from the authors.

II. EXPERIMENTAL PROCEDURE

A. Model and measurement method

Experiments were conducted in a low-speed wind tunnel of a test section of 71 cm×56 cm using a thin flexible-plate model spanning the full tunnel width, as shown in Fig. 1. The model was a 76 cm long and 1.5 mm thick Bakelite board with 38 mm long aluminum leading-edge and trailing-edge pieces. The leading-edge piece was rounded and the trailing-edge piece was sharpened to a very thin trailing edge of thickness less than 0.05 mm and tapered, with an included angle of 3°. The model was supported by five pairs of adjustable rods fixed on the ceiling and the floor near the side walls, and could be deformed into various shapes by adjusting the positions of the model-supporting brackets on the rods. Combinations of pressure gradients obtained by different shaping of the model plate and sandpaper roughness were used to manipulate the boundary-layer properties at the trailing edge. In all cases, however, the shape of the plate is made flat and parallel to the tunnel ceiling and the floor over the first and last 8 cm of the model, so that the pressure in the trailing-edge region and the downstream wake could be considered nearly constant. The resulting vertical displacement Δy of the trailing edge from the position of the leading edge was about 45 mm, as indicated in Fig. 1, which was less than 7% of the "chord" of the model. In each case, the mean velocity was measured by a pitot tube, and two fluctuating velocity components were measured by an x-array hot-wire probe operated by commercially available constant-temperature anemometers. In order to minimize the probe size effects, we have used a custom-made subminiature probe with active length of 0.6 mm and wire separation of 0.6 mm, which are smaller than commercially available probes, and a slow test velocity of 20 m/s. A static probe was also traversed to determine the variation of the mean static pressure.

TABLE I. Characteristics of boundary layers at the trailing edge.

	Symmetric	Case A	Case B	Case C
δ_{995}, upper side	20 mm	60 mm	34 mm	88 mm
δ_{995}, lower side	20 mm	12 mm	25 mm	15 mm
θ, upper side	2.4 mm	5.6 mm	3.2 mm	10.4 mm
θ, lower side	2.3 mm	1.24 mm	1.79 mm	0.92 mm
H, upper side	1.37	1.29	1.43	1.36
H, lower side	1.37	1.40	1.25	1.38
C_f, upper side	0.0035	0.0033	0.0043	0.0027
C_f, lower side	0.0036	0.0034	0.0030	0.0038
R_θ, upper side	1840	7420	4200	13800
R_θ, lower side	1840	1647	3300	1210

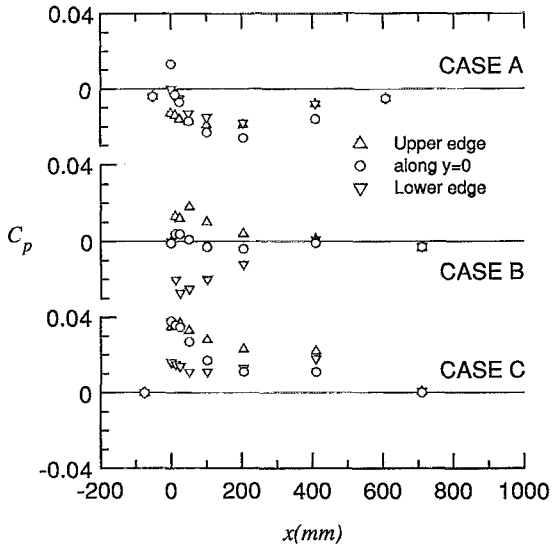

FIG. 2. Mean static pressure distributions.

B. Test flows

Three wake flows with different types of asymmetry in addition to a symmetric wake were generated, and detailed measurements were made. The free-stream velocity U_{ref} was constantly monitored and frequently adjusted during the measurements so that the Reynolds number based on the model length L and U_{ref} was within 1% of 1×10^6. The characteristics of the boundary layers at the trailing edge of all the test cases are shown in Table I. Test case A is a case in which the thickness of the boundary layers at the trailing edge are made different, but the skin-friction coefficient C_f is about the same on both sides. The velocity-profile shape parameter H, which is the ratio of the displacement thickness δ^* and the momentum thickness θ, is somewhat different but close to flat-plate values at respective Reynolds number R_θ based on the momentum thickness. In test case B, C_f and H, hence the state of the boundary layer, is made different, but keeping the boundary-layer thickness on each side as nearly equal as possible. This was a difficult case to generate, but it was achieved by delaying the transition on the upper surface, while the lower surface boundary layer was first thickened by surface roughness and then subjected to a favorable pressure gradient. The resulting boundary-layer thickness δ_{995} on the upper surface is 34 mm, which is somewhat larger than the lower surface thickness of 25 mm. In test case C, both scale and C_f are made different. This was obtained by ap-

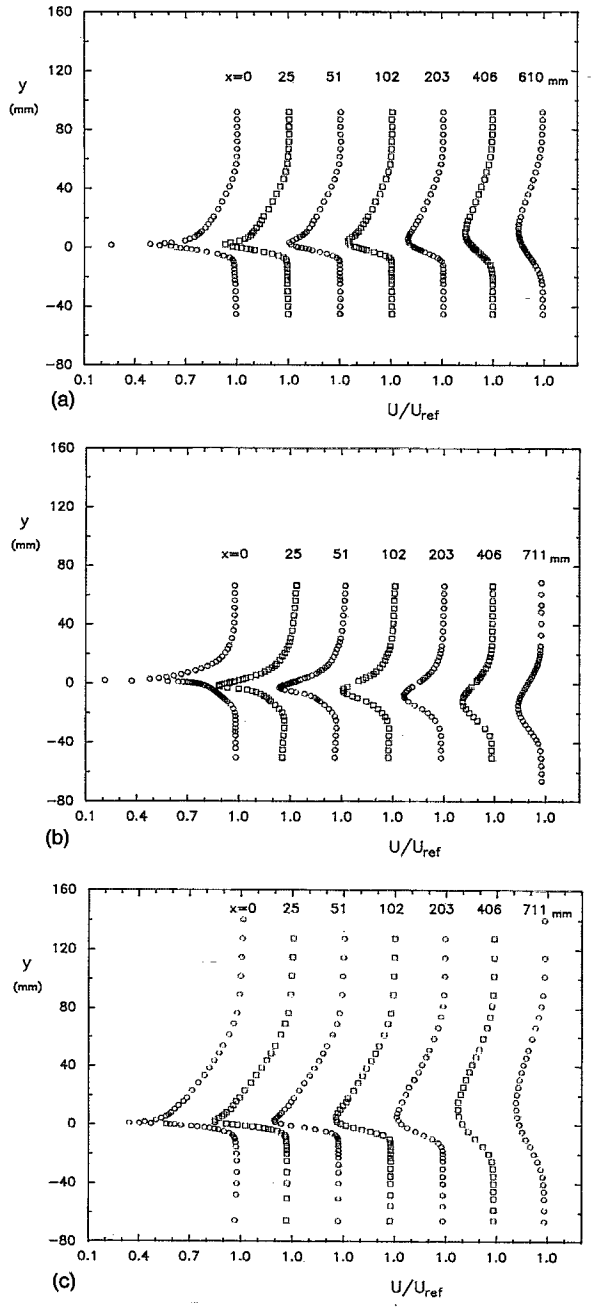

FIG. 3. Mean-velocity profiles.

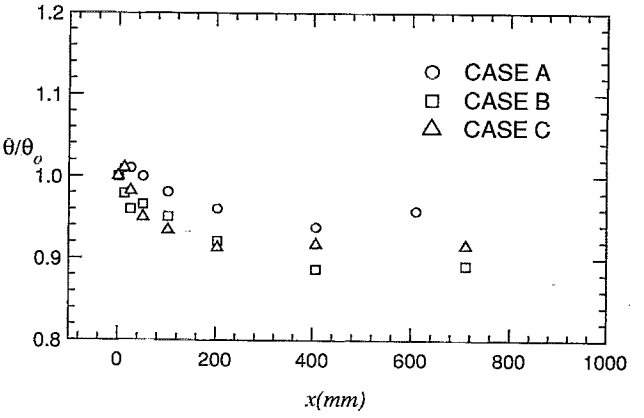

FIG. 4. Momentum thickness distributions.

plying more severe adverse pressure gradients on the upper side and favorable pressure gradients on the lower side. It turned out, as a coincidence, in this case the shape parameter H was nearly the same on both surfaces. In all cases it was ensured that there was no flow separation anywhere.

The mean static pressure variation was examined along the horizontal line passing through the trailing edge ($y=0$) and near the upper and the lower edges of the wake. The results in terms of the pressure coefficient C_p with respect to the free-stream static and dynamic pressures are shown in Fig. 2. It is seen that the total pressure variation is within 4% of the free-stream dynamic pressure. In case A, the pressure is mostly below the free-stream value and in case C is mostly above it, but in both cases the pressure gradient is negative up to about 200 mm. In case B, in which the pressure gradient on the model upstream of the trailing edge were made opposite to create the mean-velocity profiles of different shapes, the magnitude of the average streamwise pressure gradient is very small, but some transverse gradient is seen. In all test cases the magnitudes are only a few times larger than the level of pressure gradients that are unavoidably induced by the viscous displacement-thickness effects and the transverse velocity fluctuation that are found, even in the theoretical computation (Patel and Chen[9]) of the symmetric near wake of an ideally zero-thickness plate. Therefore the pressure gradient seen in the present experiments will not have a major effect to obscure the characteristics of the symmetric flows.

The mean velocity profiles normalized by the tunnel reference velocity U_{ref} in the three wakes are as in Fig. 3. The edge velocity is within a few percent of U_{ref} at all x stations, indicating again the smallness of the pressure gradient. The profiles at the last measurement station are very close to symmetry in all cases, except the last station of case A is a little closer than the other cases and some asymmetry still remains. The approach to the symmetric profile is the fastest in case B, in which a nearly symmetric profile is obtained at $x=102$ mm. The initial profile in case C appears most acute, but is seen to symmetrize faster than case A.

Figure 4 shows the variation of the momentum thickness normalized by the value θ_0 at the trailing edge. It is seen that, except for case B, the momentum thickness initially increases slightly, and then decreases thereafter in all cases. The total variation is less than 10% of the trailing-edge value, which is somewhat larger than the variation seen in the flat-plate wake measured by Andreopoulos and Bradshaw,[5] which is done at much higher Reynolds number, but not much larger than the variation found by Hayakawa and Iida,[10] who report measurements at similar Reynolds number as the present experiments in zero-pressure gradient symmetric wake. These small variations are consistent with the small favorable pressure gradient described earlier and the effects of the streamwise normal stresses.

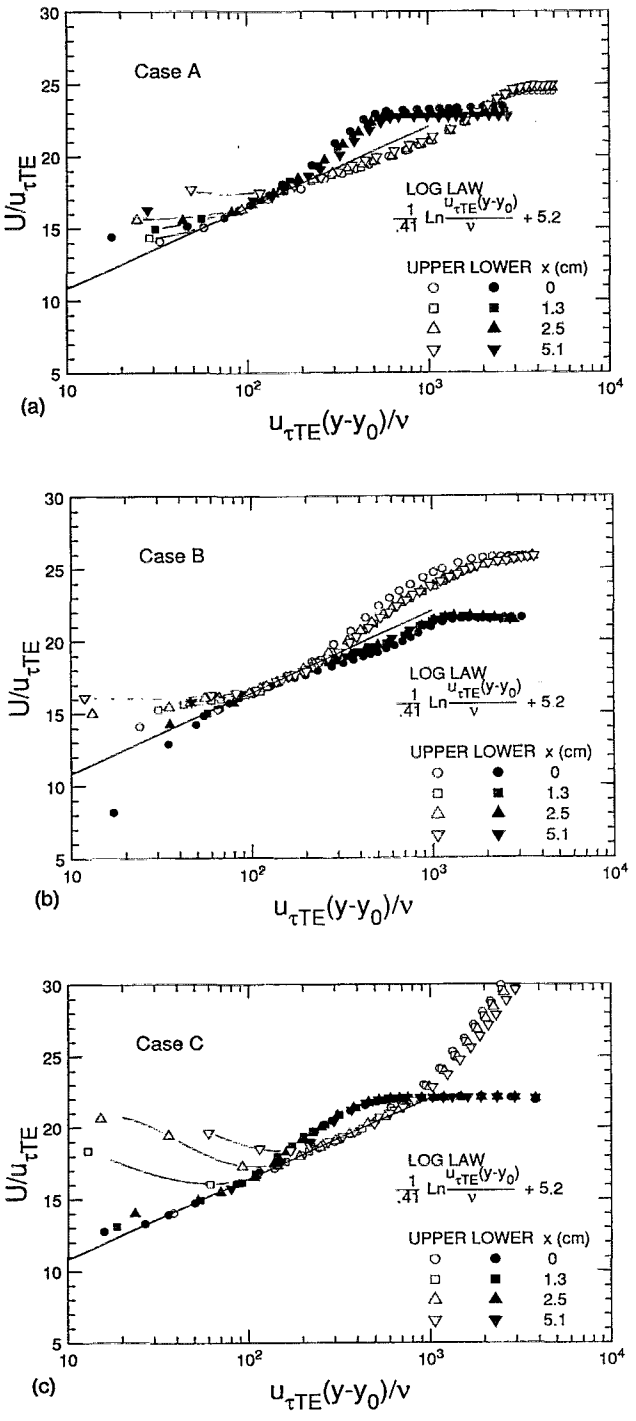

FIG. 5. Inner-law similarity in the near wake.

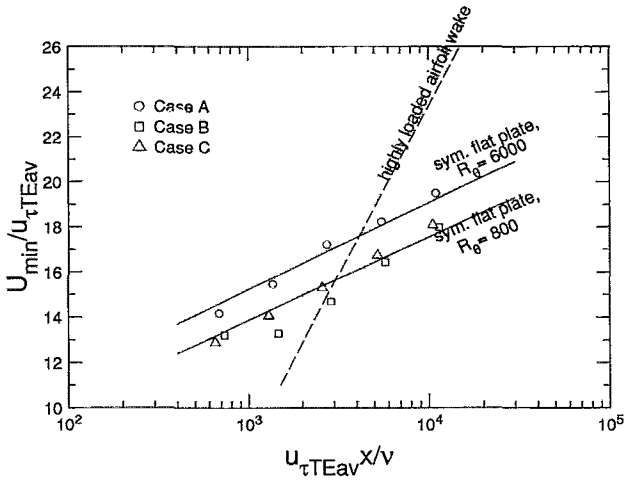

FIG. 6. Development of wake minimum velocity.

III. RESULTS AND DISCUSSION

A. Mean-velocity profiles close to the trailing edge

It is known that in symmetric wakes of flat plates, the sudden drop of the surface friction initiates the inner wake that grows within the rest of the wake, which is a continuation of the upstream boundary layers.[5,11] In the region very close to the trailing edge, where the inner wake is contained within the inner-law region of the upstream boundary layer, the logarithmic profile still exists. The velocity and the length scales of this inner-layer similarity, in the case of a symmetric flat-plate boundary layer, are the velocity and the length scales of the upstream boundary-layer wall layer. When the boundary layers are rapidly changing, like those near the trailing edge of a loaded airfoil, it is not so obvious, and it was found (Nakayama[12]) that the velocity scale changes in the streamwise distance and is some kind of weighted average of the friction velocities of the boundary layers on the two surfaces at the trailing edge. The length scale was the kinematic viscosity divided by this velocity scale, and the y origin for the log law had to be taken as the normal distance from the hypothetical wall, which is a smooth continuation of the real wall into the wake, implying that the log law is continued along the mean streamlines approximately. It is of some interest to see what kind of similarity exists in various asymmetric wakes of the present experiment.

Figures 5(a)–5(c) give the results of the similarity analysis. They represent the best similarity after trying a few different scalings. To obtain this similarity, the velocity scale is taken as the friction velocity $u_{\tau TE}$ of the boundary layer on the same side at the trailing edge. The skin friction coefficient at the trailing edge is determined using the usual Clauser method, so that the log-linear profile at $x=0$ is forced to follow the form suggested by Bradshaw, shown in the figures. The origin of y distance is taken at the extension of each model surface into the wake, y_0. For the upper side of the wake, for instance, y_0 is the position of the extension of the model upper surface. This is similar to the case of airfoils with trailing edges of finite included angle. Note that the present "flat-plate" model has a trailing edge angle of 3°. Initially the same similarity plots were tried, with the y origin taken along the horizontal line passing the trailing edge. No good similarity was obtained that way. Figure 5 shows that in all cases there is a logarithmic region corresponding to the areas downstream of the log region of the boundary layers, though it diminishes quickly in the downstream direction. If the Reynolds number was larger, the log-law region

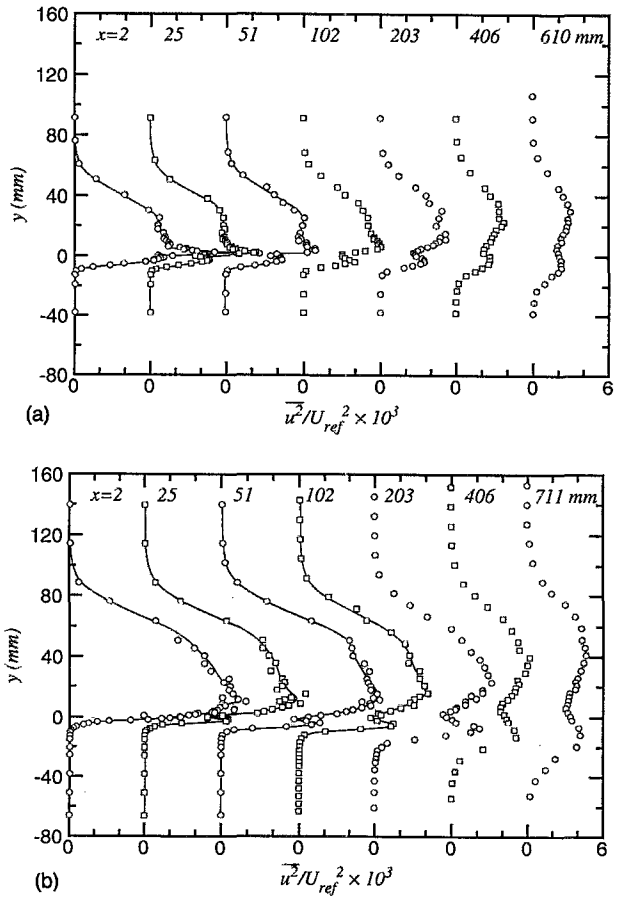

FIG. 7. Profiles of Reynolds normal stress $\overline{u^2}$.

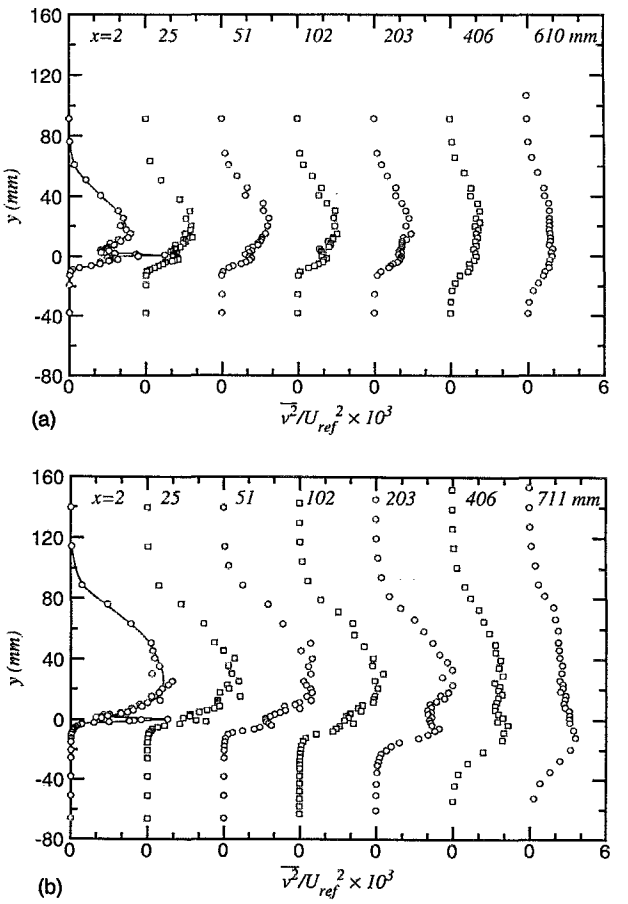

FIG. 8. Profiles of Reynolds normal stress $\overline{v^2}$.

of the boundary layers as a fraction of the boundary-layer thickness would be larger. In any case, the way the boundary layer wall similarity is continued into the wake is similar to that for an airfoil wake, except the velocity scale is constant. The pressure gradients in the wake of an airfoil with lift tend to be opposite in the upper and the lower halves and can be thought to influence the velocity scale. The constant velocity scale of the present wake flows may be said to be the result of the near constancy of pressure.

If the width of the inner wake is defined as the position where the velocity distribution near the wake center deviates from the logarithmic profile, it was verified in the symmetric near wake[11] that the thickness of this inner wake scales on the overall wake thickness rather than the inner-law length scale ν/u_τ, as implied by Andreopoulos and Bradshaw.[5] In the present data of asymmetric wakes, it is seen that the deviation from the log law is larger on the thicker side of the wake, and the minimum-velocity point moves to the same side. When the thickness is about the same on both sides (case B), the deviation from the log law is about the same on both sides. It is seen from Fig. 3(b) that in this case the position of the minimum velocity moves to the side of higher $u_{\tau TE}$. The movement of the point of the minimum velocity would, however, be more related to which side has a larger velocity defect or larger displacement thickness.

B. Development of the wake minimum velocity

In symmetric wakes of flat plate or thin airfoils, it is well demonstrated experimentally[5,10,11] and theoretically[13] that the wake minimum velocity increases logarithmically with streamwise distance. Theoretical analysis of Alber[13] indicates that this is due to the fact that the inner wake spreads in what was the logarithmic layer of the upstream boundary layer. Hence, the slope of the logarithmic increase is related to the rate of spread of the inner wake and the slope of the log law of the upstream boundary layer. In airfoil wakes, it has been seen that the slope is larger than flat-plate wakes, particularly a highly asymmetric wake downstream of a supercritical airfoil with a small trailing-edge separation, the slope was found several times larger. In the case of airfoil wake with large lift,[12] there was no log region in the boundary layer at the trailing edge, due to severe pressure gradient. It is not clear if this is due to the pressure gradient in airfoil wakes or due to the asymmetry. The present set of data show mostly the effects due to asymmetry only. Figure 6 shows that the minimum velocity $U_{\min}$ as a function of the streamwise distance, as normalized in the usual inner-law scaling. Results of symmetric flat-plate wake[11] and airfoil data[12] are also shown in the same figure for comparison. It is seen that, in cases A and C, the slope is about the same as those of symmetric flows, but the intercept is different. The reason for higher intercept for case C may be due to larger total R_θ. In

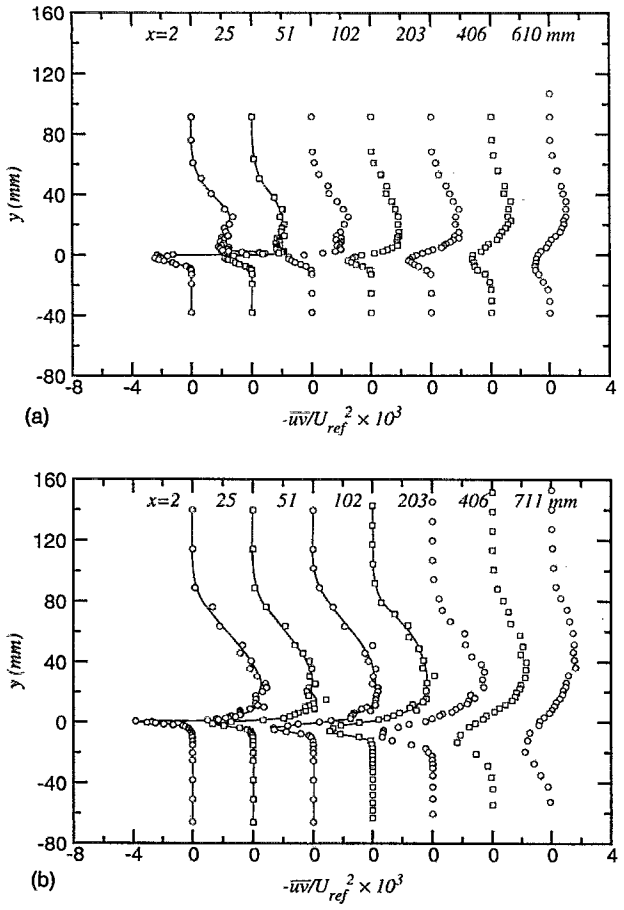

FIG. 9. Profiles of Reynolds shear stress $-\overline{uv}$.

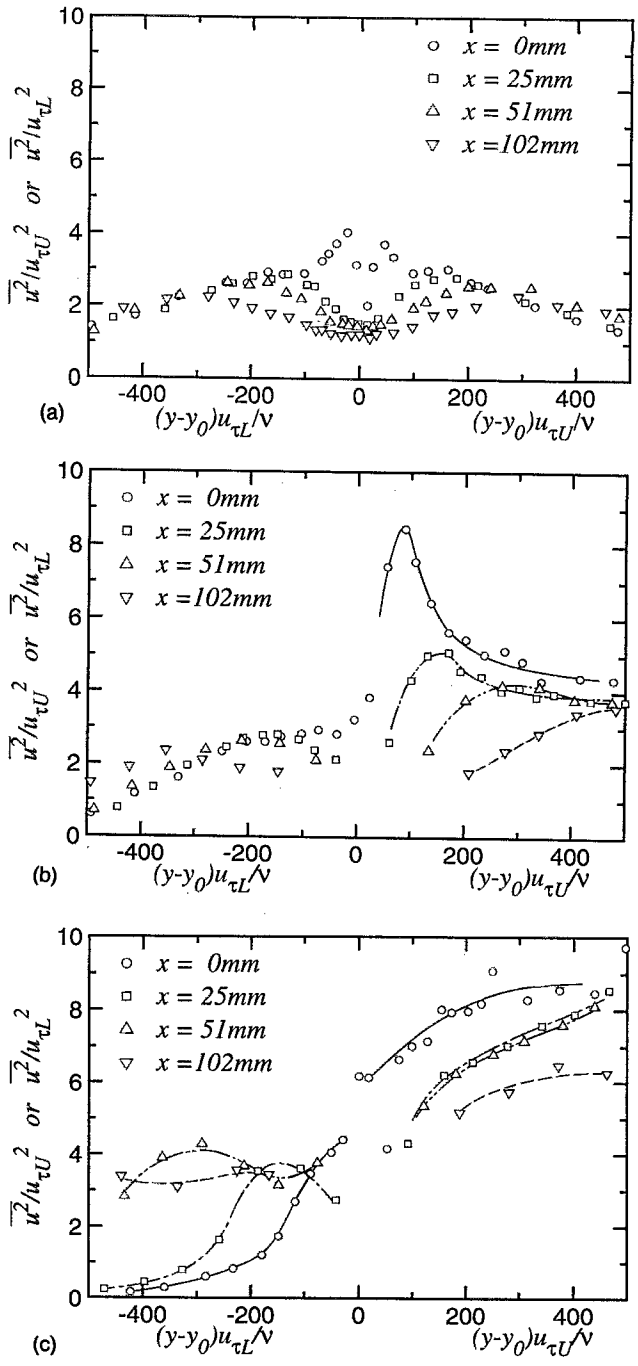

FIG. 10. Distributions of Reynolds normal stress $\overline{u^2}$ near the trailing edge.

case B, the behavior is somewhat different. The initial slope is small but becomes large downstream of approximately $xu_{\tau AV}/\nu \approx 3000$. The initial region of small increase rate corresponds to the region where the asymmetry near the wake center is very strong.

C. Reynolds stresses downstream of the trailing edge

The development of the Reynolds stress components are shown in Figs. 7–9. The first changes that occur in the Reynolds stress profiles as the boundary layers pass the trailing edge and become the wake are that the shear stress drops to zero at the centerline and then a disturbance appears in all stress profiles in the form of peaks near the centerline. There have been some arguments (Ramaprian *et al.*,[14] Haji-Haidari and Smith,[15] and Nakayama and Liu[11]) as to the cause of the peaks. Some experiments (Yu[16] and Pot[17]) show larger peaks than others. One explanation has been that they are due to small disturbances caused by a flow separation at the corner of the finite thickness trailing edge.[14] The present trailing edge is very thin (less than 0.05 mm), and it is hard to imagine a flow separation. The effects of the finite length and the separation of the hot-wire sensors were found significant when the sensor length and the separation normalized by ν/u_τ are larger than about 100 in a zero-pressure gradient boundary layer, and are to reduce $\overline{u^2}$ and to increase $\overline{v^2}$.[18] For the present sensor, they are both about 110 in the lower side of case C, in which u_τ is the largest. The peaks in $\overline{v^2}$ may be somewhat influenced by the sensor-separation effects, but these effects should be small in other cases and the other stress components. Hayakawa and Iida[10] recently concluded that the stress overshoot in the symmetric wake is an intrinsic nature of the flow in this region. Another explanation is that the slight lateral movements ("flapping") caused by the removal of the wall restriction in the region with a large velocity gradient can cause apparent turbulence. In other words, the shear production jumps but the dissipation cannot increase proportionately. A large velocity gradient means large C_f and large lateral movement is related to large

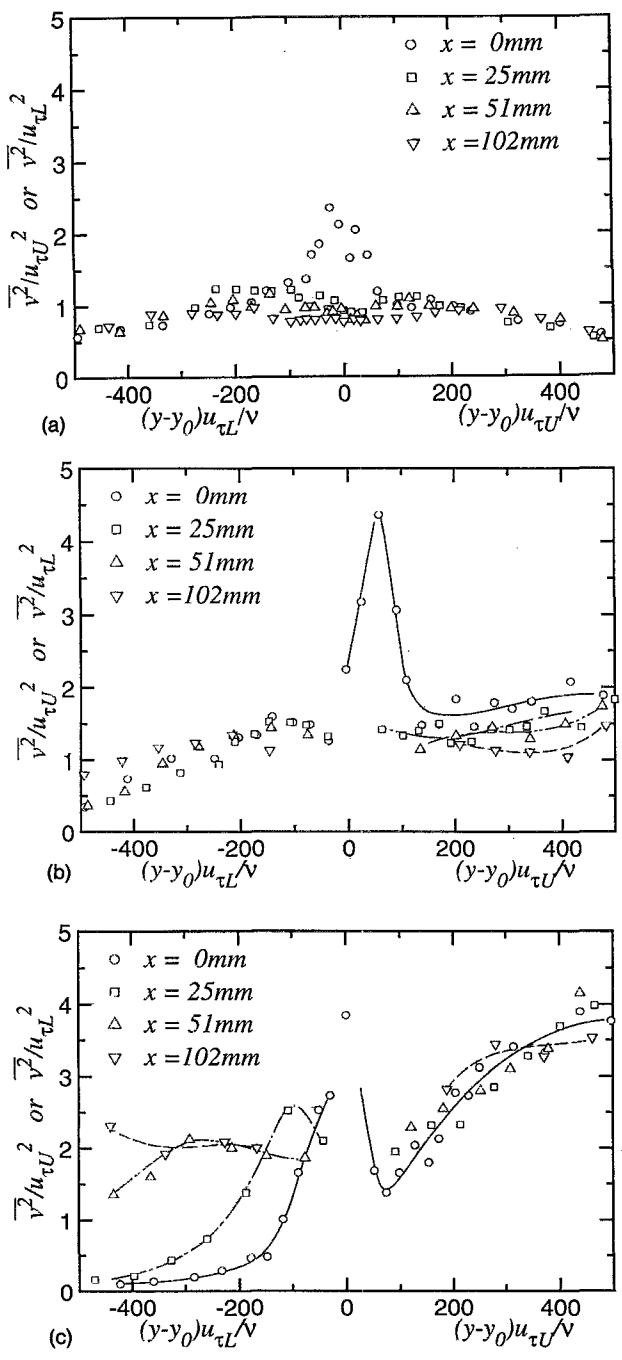

FIG. 11. Distributions of Reynolds normal stress $\overline{v^2}$ near the trailing edge.

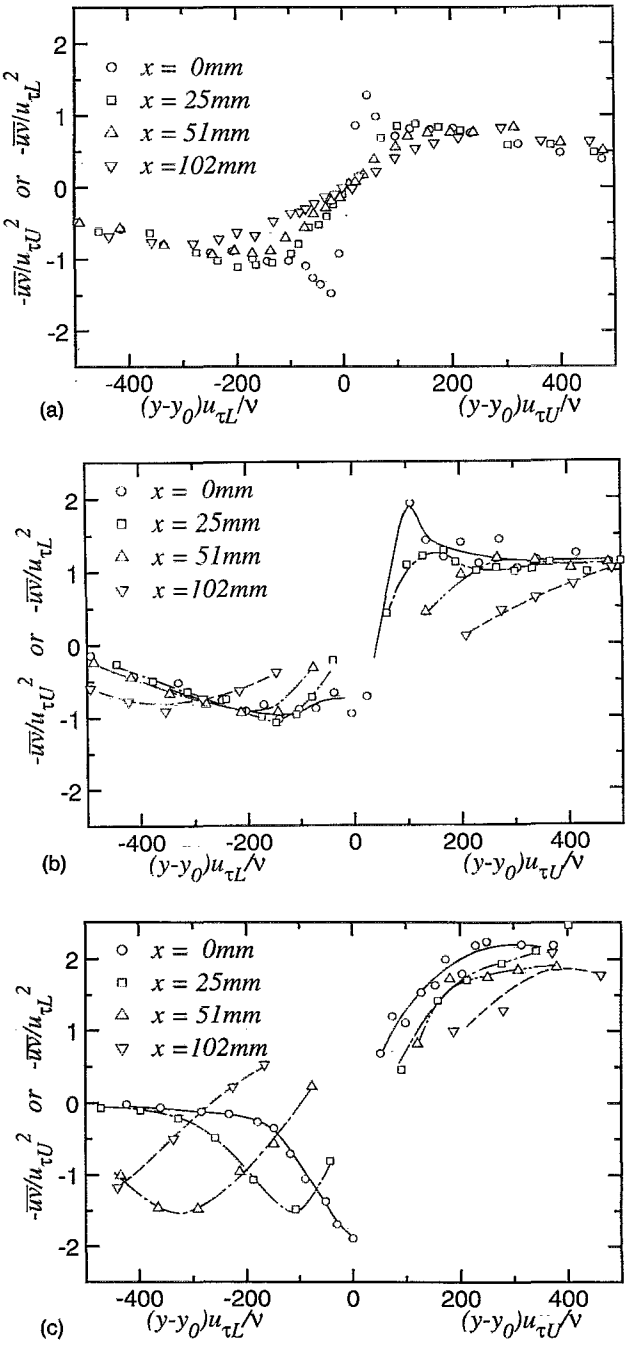

FIG. 12. Distributions of Reynolds shear stress $-\overline{uv}$ near the trailing edge.

length scale, so in asymmetric wakes, the peaks should be larger on the side of larger C_f and larger turbulence length scale. In the case of a symmetric wake, it is seen peaks of the same size appear symmetrically. In case A, where C_f is nearly the same on both sides, the peak is larger on the upper side, where the length scale is larger. In case C, where C_f is larger on the lower side but the length scale is much smaller there, the peak is slightly larger on the upper side. In all cases, the peaks appear in the region corresponding to the viscous sublayer in the upstream boundary layer, where the viscous effects suppressed the turbulence.

In order to examine similarity in the region just downstream of the trailing edge, Reynolds stress distributions in the range $yu_\tau/\nu<500$ are shown in Figs. 10–12. They are normalized by the square of the friction velocity in the boundary layer on the same side and plotted in the same extended inner-law scaling as the mean-velocity profiles so that the center region is magnified, and at the same time the similarity is examined in terms of the variables in which the mean velocity profiles were found. For each stress component, the results of the symmetric wake are shown for comparison. Note that there should be a discontinuity along $y=0$ for case C in which the C_f on the upper and lower sides are different. As to the similarity, the Reynolds stress profiles

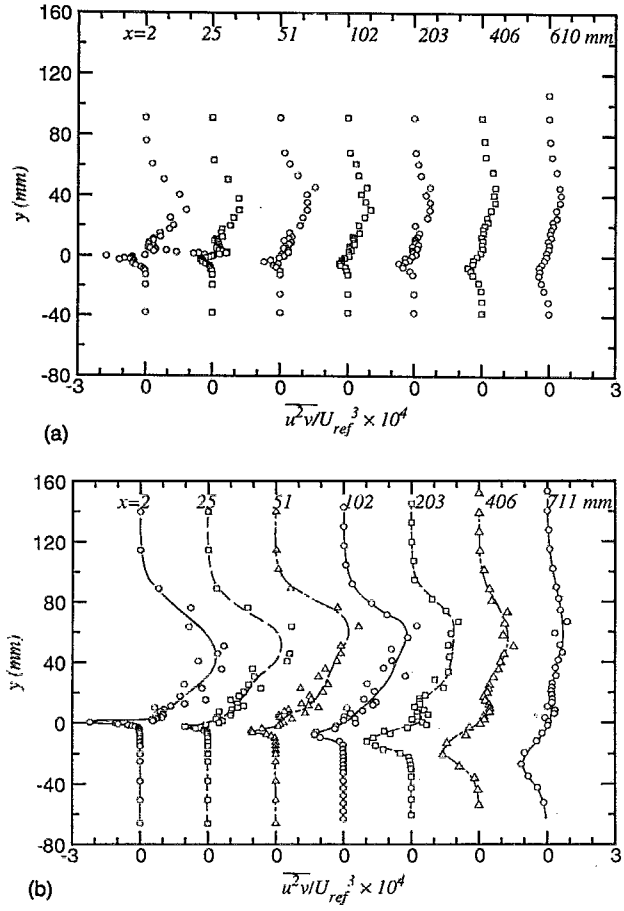

FIG. 13. Profiles of Reynolds stress transport $\overline{u^2v}$.

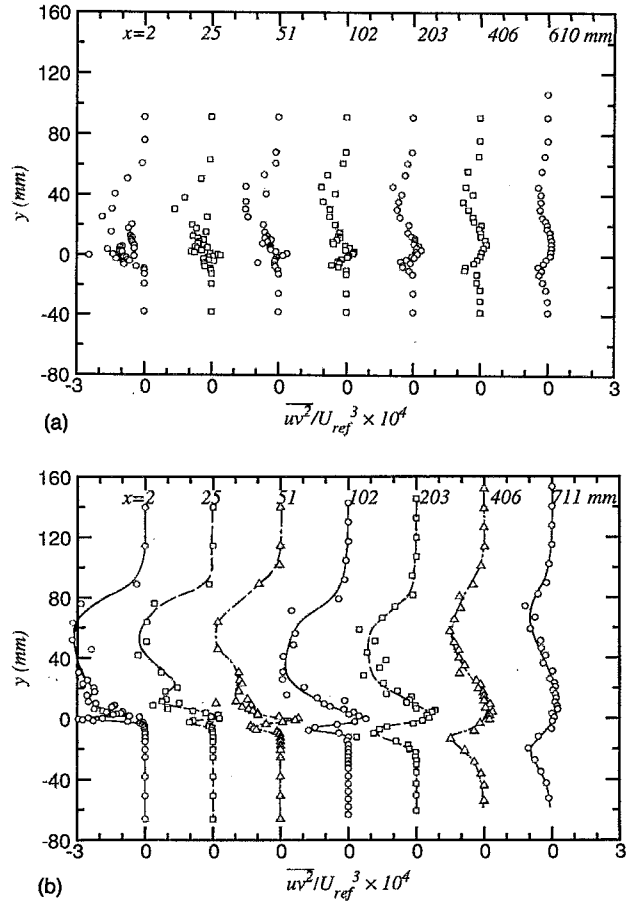

FIG. 14. Profiles of Reynolds stress transport $\overline{uv^2}$.

excluding the peaks at the initial station and their downstream development in case A show the same similarity as the symmetric wake. The shear stress distribution in the inner wake is very closely a straight line. In case C, the profiles develop rapidly and it is difficult to assess similarity.

D. Transport quantities and turbulent energy balance

The distributions of the triple products that are related to transports of the Reynolds stresses are plotted in Figs. 13–15. It is seen that case A is similar to the symmetric wake, while in the strongly asymmetric case C, the transport is large and highly asymmetric.

Figure 16 shows the turbulent kinetic energy balance at two stations for cases A and C. The first upstream station is very close to the trailing edge at $x=25$ mm and the second downstream position is at $x=205$ mm, where the stress overshoots have died but asymmetry still exists. The production terms are computed from the data without any approximation. The advection and the diffusion terms are calculated by assuming that $\overline{w^2} = \frac{1}{2}(\overline{u^2} + \overline{v^2})$ and $\overline{vw^2} = \frac{1}{2}(\overline{u^2v} + \overline{v^3})$. The contributions from the production due to the normal stresses $-(\overline{u^2} - \overline{v^2})(\partial U/\partial x)$ and the streamwise diffusion $-(\partial/\partial x)(\overline{u^3} + \overline{uv^2} + \overline{uw^2})$ are also calculated and shown in small symbols, both of which are seen to be appreciable only near $y=0$ in the upstream station, where they are negative and tend to oppose the peaks in the shear production. The dashed lines indicate the residual or the negative of the sum of advection, production, and diffusion terms. If the assumption on the quantities involving the spanwise fluctuation is acceptable and if the pressure-diffusion terms are small, the dashed lines correspond to the rate of dissipation. It is seen that this residual is positive and reasonably smooth at both stations of case A and the downstream station of case C, so it appears to represent the dissipation. At the upstream station of case C, however, it shows a negative peak near the lower edge and also a small negative peak in the outer layer on the upper side. The error due to the assumption on the spanwise fluctuation cannot be as large as this, and it is likely that the pressure diffusion is important in these regions. This is the case of asymmetry in both size and C_f. At the upstream station, it is noted that the shear production has two peaks of similar magnitude in case A, in which C_f on the upper and lower surfaces at the trailing edge are about the same. In case C, in which C_f on the lower surface is much larger than on the upper surface, there is a pronounced peak on the lower side. Although most of these production peaks are balanced by the dissipation, a significant fraction of them are seen to be taken by the transverse diffusion. The loss peaks of the diffusion term are seen to be of similar magnitude on both sides of case C, but in case A the peak is larger on the upper side, which is the thicker side. The energy budget at the downstream station of $x=203$ mm, where the rapid changes just downstream of the trailing edge have died, is qual-

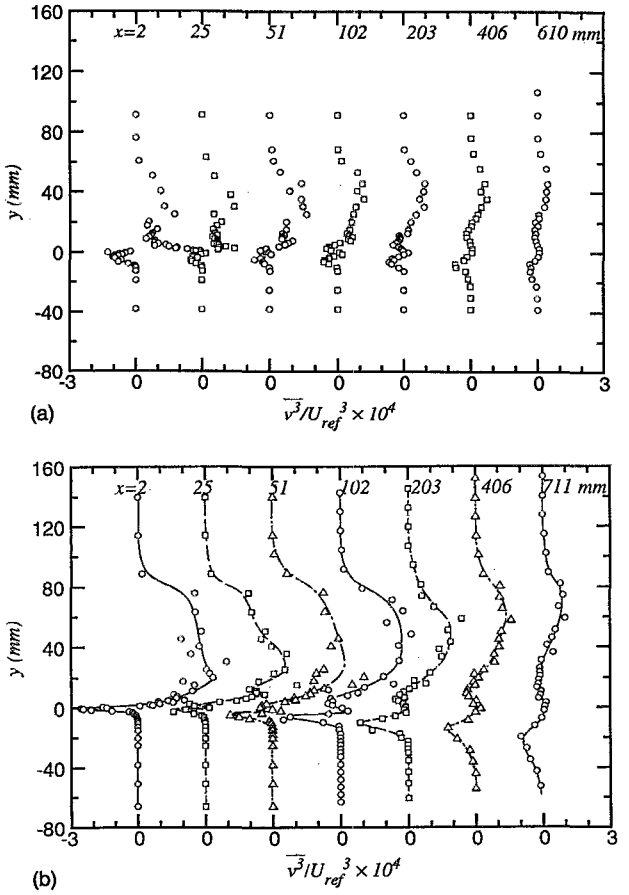

FIG. 15. Profiles of Reynolds stress transport $\overline{v^3}$.

itatively much closer between these two cases. Asymmetry in the production term is still pronounced, and most of it is now balanced by the diffusion. The dissipation here does not appear to balance the production, and even the location of maximum is shifted away from the production dominated region. It is balanced by the diffusion. This means that the energy is produced in the high shear region and transported toward the lower edge and dissipated there. This is the main mechanism in the process of symmetrizing the wake and the diffusion plays the key role in the development.

Since the diffusion is very important in asymmetric wakes, as described above, we have looked at the triple products in the light of turbulence modeling. Figure 17 shows one of the Reynolds stress components and its transport in cases A and C. They show that the sign of the transport $-\overline{u^2 v}$ is not the same as that of the gradient $\partial \overline{u^2}/\partial y$ in some regions. That region is very small for the mildly asymmetric flow of case A, but is very significant in case C. It may be said that the popular k-ϵ type model does not work very well in this case. Approaches other than the gradient type, such as the structure model of Nagano and Tagawa[19] or the nonlocal-type model, will be needed to predict highly asymmetric wakes. In fact, in Ref. 20, we have tried a diffusion model that takes into account the effects of large-scale turbulence in terms of a spatial integral and found some improvements over standard two-equation k-ϵ model.

IV. CONCLUSIONS

The characteristics of asymmetric turbulent near wakes of different types in a small pressure gradient have been

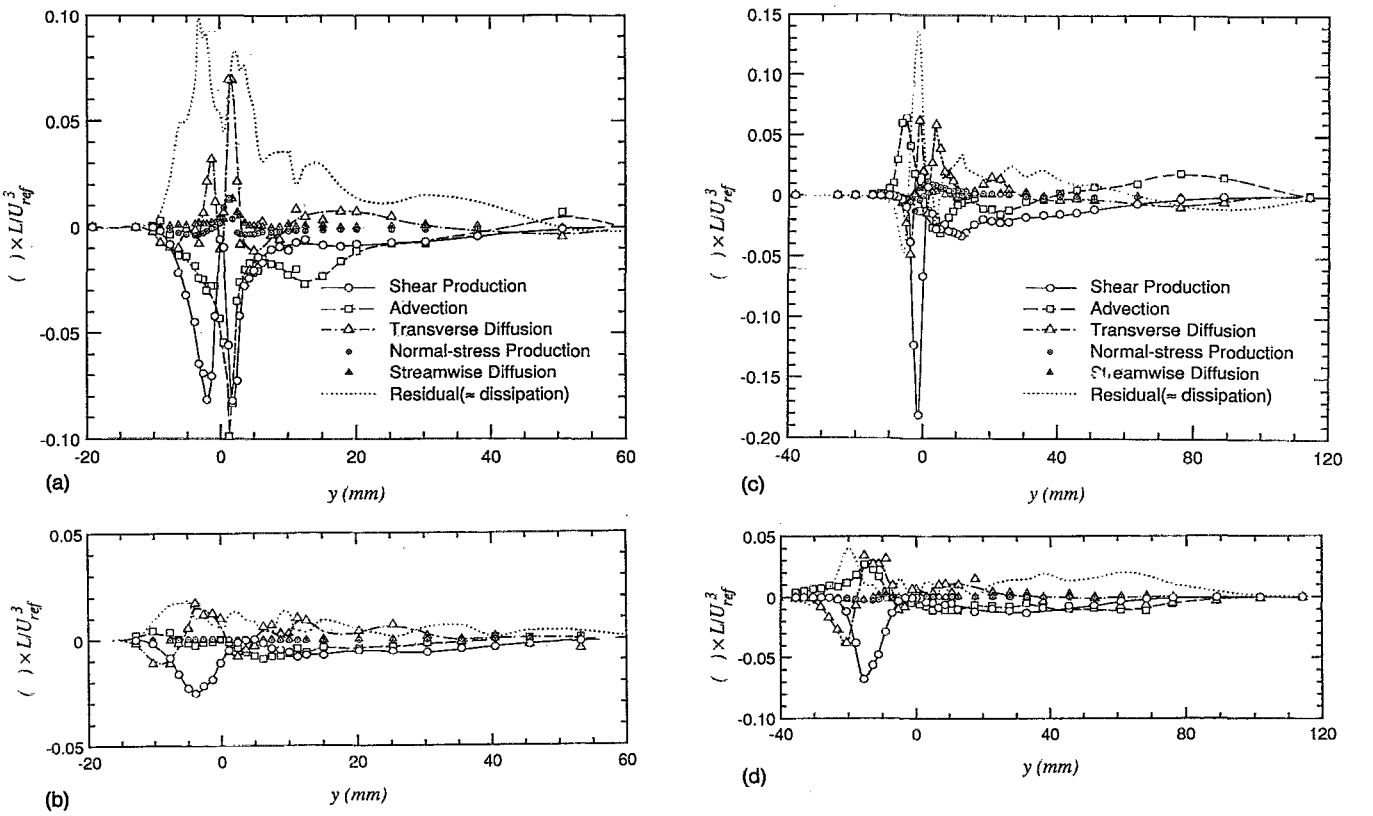

FIG. 16. Turbulent kinetic energy budget.

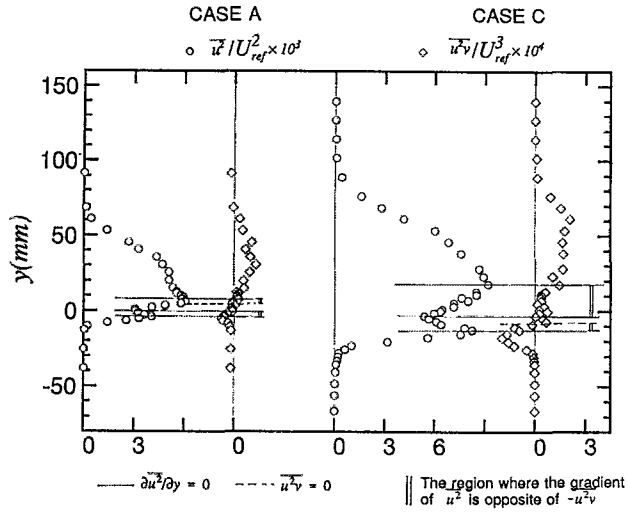

FIG. 17. Reynolds stress $\overline{u^2}$ and its transport $\overline{u^2v}$.

studied, and data have been documented. It has been found that the log-law similarity of the boundary layers continue into the initial part of the wake with the same similarity variables as in the boundary layers near the trailing edge. The Reynolds stress profiles also show the corresponding inner-law-type similarity, but contain peaks just downstream of the buffer region of the upstream boundary layer. Their magnitudes depend on the friction velocities and the length scales of the boundary layers on the two surfaces at the trailing edge. The disturbance created by the trailing edge and its diffusion are the key phenomena in the asymmetric near wake. Hence, the turbulent transport is an important element in modeling. The conventional gradient-type model fails to represent highly asymmetric cases.

ACKNOWLEDGMENTS

The experiments reported here were conducted at California State University, Long Beach. We acknowledge Mr. B. Liu for helping prepare the measurements and Mr. Saiwaki and Mr. Ikemiya of Kobe University for helping reduce the data.

[1]E. G. Tulapurkara, S. Vengadesan, and J. L. Lakshminarasimhan, "Calculation of turbulent asymmetric wake," Num. Methods Fluids **16**, 239 (1991).

[2]V. De Henau, G. D. Raithby, and B. E. Thompson, "Prediction of flows with strong curvature and pressure gradient using k-ϵ turbulence model," Trans. ASME J. Fluids Eng. **112**, 40 (1990).

[3]K. S. Kim and M. K. Chung, "Prediction of the asymmetric turbulent flow around an airfoil by k-ϵ-γ model," to appear in AIAA J.

[4]P. R. Spalart and S. R. Allmaras, "A one-equation turbulence model for aerodynamic flows," AIAA Paper No. 92-0439, 1992.

[5]A. Andreopoulos and P. Bradshaw, "Measurements of interacting turbulent shear layers in the near wake of a flat plate," J. Fluid Mech. **100**, 639 (1980).

[6]O. Leuchter, "Effects of freestream turbulence and initial boundary layers on the development of turbulent mixing layers," in *Turbulence in Internal Flows*, edited by S. N. B. Murthy (Hemisphere, Washington, DC, 1974), p. 371.

[7]B. E. Thompson and J. H. Whitelaw, "Characteristics of a trailing edge flow with turbulent boundary layer separation," J. Fluid Mech. **157**, 305 (1985).

[8]M. A. Badri Narayanan, S. Raghu, and E. G. Tulapurkara, "The nonequilibrium region of a mixing layer," AIAA J. **23**, 97 (1985).

[9]V. C. Patel and H. C. Chen, "Turbulent wake of a flat plate," AIAA J. **25**, 1078 (1987).

[10]M. Hayakawa and S. Iida, "Behavior of turbulence in the near wake of a thin flat plate at low Reynolds numbers," Phys. Fluids A **4**, 2282 (1992).

[11]A. Nakayama and B. Liu, "The turbulent near wake of a flat plate at low Reynolds number," J. Fluid Mech. **217**, 93 (1990).

[12]A. Nakayama, "Characteristics of the flow around conventional and supercritical airfoils," J. Fluid Mech. **160**, 155 (1985).

[13]I. E. Alber, "Turbulent wake of a thin flat plate," AIAA J. **18**, 1044 (1980).

[14]B. R. Ramaprian, V. C. Patel, and M. S. Sastry, "The symmetric turbulent wake of a flat plate," AIAA J. **20**, 1228 (1982).

[15]A. Haji-Haidari and C. R. Smith, "Development of the turbulent near wake of a tapered thick flat plate," J. Fluid Mech. **189**, 135 (1988).

[16]J. C. Yu, "Mean-flow and turbulence measurements in the vicinity of the trailing edge of an NACA 631-012 airfoil," NASA TP 1845, 1981.

[17]P. J. Pot, "Measurements in a 2-D wake and in a 2-D wake merging into a boundary layer with zero pressure gradient," NTR TR-7900638, The Netherlands, 1979.

[18]A. Nakayama and R. V. Westphal, "The effects of sensor length and spacing on X-wire measurements in a boundary layer," NASA TM88352, 1986.

[19]Y. Nagano and M. Tagawa, "A structural turbulence model for triple products of velocity and scalar," J. Fluid Mech. **215**, 639 (1990).

[20]A. Nakayama and S. Vengadesan, "A nonlocal turbulent transport model," *Proceedings of the 9th Symposium on Turbulent Shear Flows*, 1993, p. 26-4.